Monthly Notices
of the
ROYAL ASTRONOMICAL SOCIETY

Mon. Not. R. Astron. Soc. **414,** 3023–3035 (2011) doi:10.1111/j.1365-2966.2011.18603.x

The spin-orbit angles of the transiting exoplanets WASP-1b, WASP-24b, WASP-38b and HAT-P-8b from Rossiter–McLaughlin observations⋆

E. K. Simpson,[1]† D. Pollacco,[1] A. Collier Cameron,[2] G. Hébrard,[3,4] D. R. Anderson,[5] S. C. C. Barros,[1] I. Boisse,[3] F. Bouchy,[3,4] F. Faedi,[1] M. Gillon,[6] L. Hebb,[7] F. P. Keenan,[1] G. R. M. Miller,[2] C. Moutou,[8] D. Queloz,[9] I. Skillen,[10] P. Sorensen,[11] H. C. Stempels,[12] A. Triaud,[9] C. A. Watson[1] and P. A. Wilson[11,13]

[1]*Astrophysics Research Centre, School of Mathematics & Physics, Queen's University Belfast, Belfast BT7 1NN*
[2]*School of Physics and Astronomy, University of St Andrews, North Haugh, St Andrews, Fife KY16 9SS*
[3]*Institut d'Astrophysique de Paris, UMR7095 CNRS, Université Pierre & Marie Curie, France*
[4]*Observatoire de Haute-Provence, CNRS/OAMP, 04870 St Michel l'Observatoire, France*
[5]*Astrophysics Group, Keele University, Staffordshire ST5 5BG*
[6]*Université de Liège, Allée du 6 août 17, Sart Tilman, Liège 1, Belgium*
[7]*Department of Physics and Astronomy, Vanderbilt University, Nashville, TN 37235, USA*
[8]*Laboratoire d'Astrophysique de Marseille, 38 rue Frédéric Joliot-Curie, 13388 Marseille Cedex 13, France*
[9]*Observatoire de Genève, Université de Genève, 51 Ch. des Maillettes, 1290 Sauverny, Switzerland*
[10]*Isaac Newton Group of Telescopes, Apartado de Correos 321, E-38700 Santa Cruz de la Palma, Spain*
[11]*Nordic Optical Telescope, Apartado de Correos 474, E-387 00 Santa Cruz de la Palma, Canary Islands, Spain*
[12]*Department of Physics and Astronomy, Uppsala University, Box 516, SE-751 20 Uppsala, Sweden*
[13]*Astrophysics Group, School of Physics, University of Exeter, Stocker Road, Exeter EX4 4QL*

Accepted 2011 February 24. Received 2011 February 6; in original form 2010 November 25

ABSTRACT

We present observations of the Rossiter–McLaughlin effect for the transiting exoplanets WASP-1b, WASP-24b, WASP-38b and HAT-P-8b, and deduce the orientations of the planetary orbits with respect to the host stars' rotation axes. The planets WASP-24b, WASP-38b and HAT-P-8b appear to move in prograde orbits and be well aligned, having sky-projected spin-orbit angles consistent with zero: $\lambda = -4.^{\circ}7 \pm 4.^{\circ}0$, $15^{\circ}{}^{+33}_{-43}$ and $-9.^{\circ}7^{+9.0}_{-7.7}$, respectively. The host stars have $T_{\rm eff} < 6250$ K and conform with the trend of cooler stars having low obliquities. WASP-38b is a massive planet on a moderately long period, eccentric orbit so may be expected to have a misaligned orbit given the high obliquities measured in similar systems. However, we find no evidence for a large spin-orbit angle. By contrast, WASP-1b joins the growing number of misaligned systems and has an almost polar orbit, $\lambda = -79.^{\circ}0^{+4.5}_{-4.3}$. It is neither very massive, eccentric nor orbiting a hot host star, and therefore does not share the properties of many other misaligned systems.

Key words: techniques: radial velocities – stars: individual: WASP-1 – stars: individual: WASP-24 – stars: individual: WASP-38 – stars: individual: HAT-P-8 – planetary systems.

1 INTRODUCTION

The process of exoplanet migration has been a hotly debated topic since the first close-in planets were discovered (Mayor & Queloz 1995; Butler & Marcy 1996; Marcy & Butler 1996). We are able to explore the mechanisms which move planets inwards from large orbits through a statistical analysis of their dynamical properties such as orbital period, eccentricity and spin-orbit alignment. In particular, transiting planets allow us to measure the sky-projected angle (λ) between the stellar rotation axis and planetary orbit through measurement of the Rossiter–McLaughlin (RM) effect (McLaughlin

⋆This work is based on observations collected with the SOPHIE spectrograph on the 1.93-m telescope at Observatoire de Haute-Provence (CNRS), France, by the SOPHIE Consortium; the Nordic Optical Telescope, operated on the island of La Palma jointly by Denmark, Finland, Iceland, Norway and Sweden, in the Spanish Observatorio del Roque de los Muchachos of the Instituto de Astrofisica de Canarias and the HARPS spectrograph mounted on the European Southern Observatory (ESO) 3.6-m telescope at the La Silla Observatory in Chile under proposal 084.C-0185.

†E-mail: esimpson05@qub.ac.uk

1924; Rossiter 1924). The effect is caused by the planet sequentially passing over and blocking portions of the rotating stellar surface resulting in a radial velocity (RV) shift which traces the trajectory of the planet across the stellar disc and allows the orbital obliquity to be estimated.

The first measurements of λ found the systems to be well aligned and suggested that the planets had lost orbital angular momentum through interactions with the protoplanetary disc (Lin, Bodenheimer & Richardson 1996; Murray et al. 1998). However, there are now a growing number of planets with highly misaligned and even retrograde orbits which now make up approximately one-third of the systems so far studied. Several theories have been postulated to explain this. For example, it has been suggested that protoplanetary discs may not always be aligned with the stellar rotation axis as previously assumed (Bate, Lodato & Pringle 2010; Lai, Foucart & Lin 2011), although Watson et al. (2010b) found no evidence for misaligned debris discs in eight systems. Fabrycky & Winn (2009) and Triaud et al. (2010) suggest that another, more dynamically violent process involving interactions with a third body (another planet or star) causes the misaligned orbits (see Rasio & Ford 1996; Wu & Murray 2003; Nagasawa, Ida & Bessho 2008). Whether a single mechanism or a combination of several is at work remains to be tested by increasing the number of measured systems. Interestingly, the fraction of aligned systems in binary stars appears to be higher than that for planets, which demonstrates the differences between the two configurations (see Albrecht et al. 2011 for a summary of results).

Misaligned planetary systems appear to be synonymous with eccentricity; six of the eight eccentric planets with measured spin-orbit angles are reported to have obliquities significantly different from zero: XO-3b (Hébrard et al. 2008), HD 80606b (Gillon 2009; Moutou et al. 2009; Pont et al. 2009; Winn et al. 2009), WASP-8b (Queloz et al. 2010), WASP-14b (Johnson et al. 2009), HAT-P-11b (Winn et al. 2010b), HAT-P-14b (Winn et al. 2011), with HAT-P-2b (Loeillet et al. 2008) and HD 17156b (Narita et al. 2009) being the exceptions. Although HD 17156b does not show a large sky-projected misalignment, Schlaufman (2010) notes that the stellar rotation axis may be tilted along the line of sight. Another trend, noted by Johnson et al. (2009), is the correlation between planet mass and misalignment. Hébrard et al. (2010) suggests that there could be several populations of planets, with those more massive than Jupiter undergoing a different migration scenario leading to the high spin-orbit angles. Winn et al. (2010a) and Schlaufman (2010) find that misaligned orbits are more common in host stars with larger masses/higher effective temperatures. It is suggested that the tidal torques experienced by cooler stars, with deeper convective zones, could cause their envelopes to quickly align with a planet's orbit, thereby erasing any initial misalignment. Exceptions to this effect may be longer period and low-mass planets which experience weaker tidal forces and therefore longer tidal timescales.

We present spectroscopic observations of the transiting planets WASP-1b (Cameron et al. 2007), WASP-24b (Street et al. 2010), WASP-38b (Barros et al. 2011) and HAT-P-8b (Latham et al. 2009) obtained using the HARPS, SOPHIE and FIES spectrographs to determine their spin-orbit alignments. All the host stars are of similar temperature, $\sim$6100 K, but have diverse physical and dynamical properties which allows us to investigate possible trends independent of $T_{\rm eff}$. WASP-1b, WASP-24b and HAT-P-8b are non-eccentric, short-period planets (2.3–3.1 d) with masses similar to Jupiter (0.9–1.5 $M_{\rm J}$), whereas WASP-38b is a massive planet on a moderately longer period orbit with a small but significant eccentricity ($m_{\rm p} = 2.7\,M_{\rm J}$, $P = 6.9$ d, $e = 0.032^{+0.0050}_{-0.0044}$, Barros et al. 2011).

In Section 2, we describe the general data analysis procedures and methods performed to measure the spin-orbit angles. The derived parameters for the four systems are presented in Section 3, and the implications of these are discussed in Section 4.

2 DATA ANALYSIS

2.1 Radial velocity extraction

The data presented in this paper were obtained using three spectrographs: HARPS, SOPHIE and FIES; the instrumental setup and data reduction for each is described in this section. Details of the individual observations and results of each system are discussed in Section 3.

2.1.1 HARPS

The HARPS instrument is a high-resolution ($R = 110\,000$) stabilized echelle spectrograph mounted at the La Silla 3.6-m European Southern Observatory (ESO) telescope. Observations were conducted in the OBJO mode without simultaneous Thorium–Argon (ThAr) calibration. The wavelength solution was calculated using a ThAr calibration at the start of the night, and HARPS is stable within 1 m s^{-1} across a night (Rupprecht et al. 2004), which is much lower than the photon noise on the data points. Spectra were extracted and cross-correlated against a template of a G2V-type star using the HARPS data reduction software (DRS) (see Baranne et al. 1996; Pepe et al. 2002; Mayor et al. 2003; Lovis & Pepe 2007 for more details).

2.1.2 SOPHIE

SOPHIE is a cross-dispersed, environmentally stabilized echelle spectrograph (wavelength range 3872.4–6943.5 Å) designed for high-precision RV measurements. The spectrograph was used in high-efficiency mode (resolution $R = 40\,000$) with the CCD in slow readout mode to reduce the readout noise. Two 3-arcsec diameter optical fibres were used: the first centred on the target and the second on the sky to simultaneously measure its background in case of contamination from scattered moonlight. The spectra were reduced using the SOPHIE pipeline (Perruchot et al. 2008). Radial velocities were computed from a weighted cross-correlation of each spectrum with a numerical mask of G2V spectral type. A Gaussian was fitted to the cross-correlation functions to obtain the RV shift, and the uncertainty was computed using the empirical relation given by Bouchy et al. (2009) and Cameron et al. (2007).

2.1.3 FIES

The FIES spectrograph is mounted on the 2.5-m Nordic Optical Telescope on La Palma. FIES was used in medium-resolution mode ($R = 46\,000$) with simultaneous ThAr calibration. Care was taken to select nights in which the moon was greater than 60° from the target to avoid contamination from scattered light. Spectra were extracted using the bespoke data reduction package FIEStool.[1] An

[1] http://www.not.iac.es/instruments/fies/fiestool/FIEStool.html

IDL cross-correlation routine was used to obtain the radial velocities by finding the maximum of the cross-correlation functions of 30 spectral orders and taking the mean.

A template spectrum was constructed by shifting and co-adding the out-of-transit spectra, against which the individual spectra were cross-correlated to obtain the final velocities. This template was cross-correlated with a high signal-to-noise ratio (S/N) spectrum of the Sun to obtain the absolute velocity to which the relative RVs were shifted. We estimated the RV uncertainty by $\sigma = \mathrm{rms}(v)/\sqrt{N}$, where v is the RV of the individual orders and N is the number of orders.

When fitting the data, we found that the FIES observations have a reduced $\chi^2_{\mathrm{red}} = \chi^2/\mathrm{d.o.f.} > 1$ (d.o.f. = number of points − number of fitted parameters). This suggests that there is an extra source of noise present, which has not been accounted for in the internal errors. The cause may be that the ThAr calibration does not travel through the same light path as the stellar light (Buchhave et al. 2010), or that because the fibre lacks a scrambler there is a non-uniform illumination of the spectrograph (Queloz et al. 1999). To account for these instrumental effects, 15 m s^{-1} of uncorrelated noise was added in quadrature to the internal error estimation to obtain a reduced χ^2 value of unity. The photon errors are given in the data tables, whereas the rescaled uncertainties are shown in the figures.

2.2 Model fitting

The RM effect and orbit were fitted simultaneously using all the available spectroscopic data. A Keplerian model was used for the orbit, and the analytical approach described in Ohta, Taruya & Suto (2005) was used to calculate the RM effect. We refer the reader to this paper for a detailed description of the model. The equations were modified to make them dependent on R_{p}/R_* and a/R_*, rather than on R_{p}, R_* and a, to reflect the parameters derived from photometry and to reduce the number of free parameters.

We modelled the RM velocity anomaly as $v_{\mathrm{RM}} = -\delta v_{\mathrm{p}}/(1-\delta)$, where δ is the flux blocked by planet $\sim(R_{\mathrm{p}}/R_*)^2$ and v_{p} is the subplanet velocity, i.e. the velocity component of the rotating stellar surface blocked by the planet $\sim x_{\mathrm{p}}\, v \sin i/R_*$, where x_{p} is the x coordinate of the position of the planet on the stellar surface (see fig. 5 of Ohta et al. 2005).

In brief, the model comprises the following parameters: the orbital period, P; mid-transit time (in the UTC system), T_0; planetary-to-stellar radius ratio, R_{p}/R_*; scaled semimajor axis, a/R_*; orbital inclination, i; orbital eccentricity, e; longitude of periastron, ω; RV semi-amplitude, K; sky-projected angle between the stellar rotation axis and orbital angular momentum vector, λ; projected stellar rotational velocity, $v \sin i$; the stellar linear limb-darkening coefficient, u; and the systemic velocity of orbital data set, γ. To allow for instrumental offsets, a different systematic velocity was assigned to each orbital data set. The transit data sets were also fitted with separate systematic velocities to allow for any shift in velocity zero-point due to long-term stellar activity or instrumental variations. A linear limb-darkening law was assumed, as the quadratic law alters the model by only a few m s^{-1} and so does not seem justified given the precision of the RM data. As a test, u was left as a free parameter and no significant effect on λ or $v \sin i$ was found.

Some parameters have been tightly constrained by previous observations (e.g. P, R_{p}/R_*). We use this information in the form of a penalty function on the χ^2 statistic:

$$\chi^2 = \sum_i \left[\frac{v_{i,\mathrm{obs}} - v_{i,\mathrm{calc}}}{\sigma_i}\right]^2 + \left(\frac{A - A_{\mathrm{obs}} + \sigma_{A_{\mathrm{obs}}} \times G(0,1)}{\sigma_{A_{\mathrm{obs}}}}\right)^2, \quad (1)$$

where $v_{i,\mathrm{obs}}$ and $v_{i,\mathrm{calc}}$ are the ith observed and calculated radial velocities and σ_i is the corresponding observational error. A is a fitted parameter, A_{obs} is the parameter value determined from other observations and $\sigma_{A_{\mathrm{obs}}}$ is the uncertainty in A_{obs}. The value $G(0, 1)$ is a Gaussian randomly generated number of mean = 0 and standard deviation = 1. This allows the uncertainty in A_{obs} to be accounted for in the error budget. Depending on the situation, several penalty functions were used to constrain parameters in the fit, and these are described in the individual analyses. If a parameter has asymmetric uncertainties, we have adopted the larger error.

Best-fitting parameters were obtained by minimizing the χ^2 statistic using the IDL-based MPFIT function (Markwardt 2009), a least-squares minimization technique using the Levenberg–Marquardt algorithm. The 1σ best-fitting parameter uncertainties were calculated using a Monte Carlo method. We created 10^5 synthetic data sets by adding a 1σ Gaussian random variable to the data points. The free parameters were re-optimized for each simulated data set to obtain the distribution of the parameter values. These distributions were not assumed to be Gaussian and the 1σ limits were found from the 15.85 and 84.15 per cent bounds.

3 ANALYSIS

3.1 WASP-1

A transit of WASP-1b was observed with the SOPHIE spectrograph at the 1.93-m telescope at Haute-Provence Observatory on the night of 2009 September 24. We acquired 21 spectra of WASP-1 covering the full transit (224 min, 12 observations) and a period of duration 156 min (nine observations) post-transit. No observations were possible prior to transit due the low altitude of the target at this time. The exposure time was adjusted between 13 and 22 min in order to reach a constant S/N of 30 at 550 nm. Moon illumination was 39 per cent and at a distance of $>115^\circ$, so this did not significantly affect the RV determination.

To fit the orbit, we used seven SOPHIE observations obtained during the discovery of the planet (Cameron et al. 2007) and 16 FIES spectra taken at various orbital phases between 2009 January 1 and September 27. The new SOPHIE and FIES observations are shown in Table 1. Wheatley et al. (2010) observed a secondary eclipse of WASP-1b and found that the eccentricity was consistent with zero, and in the models, e has been set to 0 accordingly. The linear limb-darkening coefficient was chosen from the tables of Claret (2004) (ATLAS models) for the g' filter and fixed at $u = 0.73$.

A significant period of time has passed since the discovery of WASP-1b in 2006 and the orbital ephemeris may have drifted, leading to an inaccurate determination of the mid-transit time. To update the ephemeris, we fitted the z-band light curve presented in Charbonneau et al. (2007), the full I-band transit from Shporer et al. (2007) and a high-quality light curve taken on 2010 August 26 by

Table 1. Radial velocities of WASP-1 measured with SOPHIE during transit and FIES at other orbital phases.

BJD − 240 0000	RV (km s^{-1})	Error (km s^{-1})
Planetary transit		
55099.33177	−13.2101	0.0083
55099.34602	−13.2153	0.0086
55099.35950	−13.2128	0.0087
55099.37319	−13.2040	0.0086
55099.38674	−13.2146	0.0086
55099.40012	−13.2218	0.0085
55099.41520	−13.2341	0.0085
55099.42765	−13.2228	0.0085
55099.43928	−13.2454	0.0086
55099.45150	−13.2457	0.0087
55099.46349	−13.2614	0.0087
55099.47532	−13.2671	0.0088
55099.48773	−13.2527	0.0092
55099.50089	−13.2662	0.0088
55099.51269	−13.2596	0.0083
55099.52912	−13.2711	0.0072
55099.54277	−13.2774	0.0081
55099.55493	−13.2635	0.0086
55099.56709	−13.2843	0.0087
55099.58288	−13.2739	0.0088
55099.59579	−13.2883	0.0087
HJD − 240 0000	RV (km s^{-1})	Error (km s^{-1})
Other orbital phases		
54834.3378	−13.3780	0.0105
54835.4419	−13.6246	0.0107
54836.4229	−13.4224	0.0096
55025.7036	−13.4250	0.0191
55041.6483	−13.5199	0.0249
55085.5576	−13.5266	0.0154
55086.5259	−13.4365	0.0393
55087.4126	−13.6088	0.0223
55096.5906	−13.4449	0.0215
55097.6051	−13.6009	0.0181
55098.5769	−13.4039	0.0223
55099.6120	−13.5478	0.0125
55100.5339	−13.5002	0.0102
55119.4279	−13.4457	0.0131
55119.6984	−13.5493	0.0187

F. Harmuth as part of the TRESCA/ETD project[2] (Poddaný, Brát & Pejcha 2010), as shown in Fig. 1. The TRESCA transit was observed using the 1.2-m telescope at Calar Alto observatory, Spain, using an *R*-band filter. A Markov Chain Monte Carlo (MCMC) routine was used to fit the data (see Cameron et al. 2007 and Pollacco et al. 2008 for more details). The non-linear limb-darkening coefficients were chosen for the appropriate stellar temperature and photometric passband for each light curve. The parameters found for P, T_0, R_p/R_*, a/R_* and i_p were used to constrain the fit in the form of penalty functions and are shown in equation (2).

WASP-1b has a low impact parameter, $b < 0.2$, and in this regime $v \sin i$ and λ are highly correlated. The shape of the RM signal is not strongly dependent on λ, whereas the amplitude is dependent

[2] http://var2.astro.cz/EN/tresca/

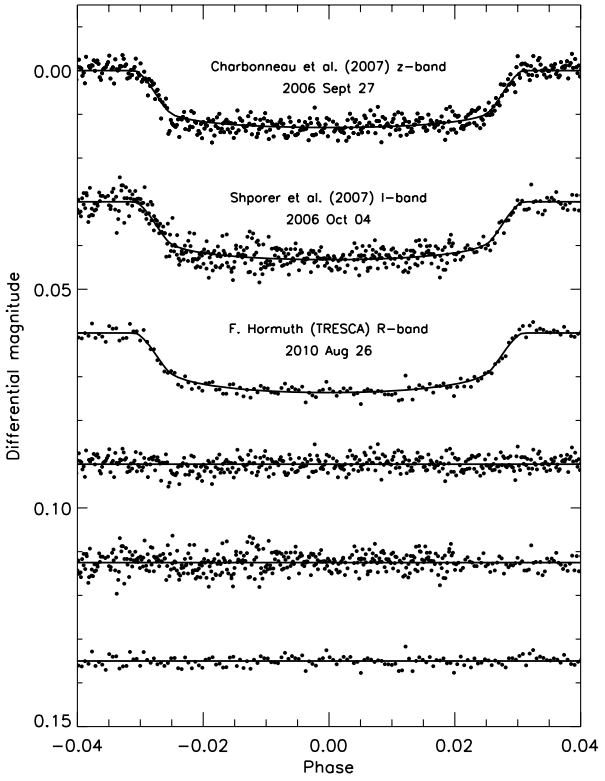

Figure 1. Top panel: photometry of three transits of WASP-1b and the residuals from the best-fitting model.

on both $v \sin i$ and λ. To break this degeneracy, we introduced a penalty function on $v \sin i$ using the value of 5.79 ± 0.35 km s^{-1} found from spectroscopic line-broadening measurements by Stempels et al. (2007). The following χ^2 statistic was adopted:

$$\chi^2 = \sum_i \left[\frac{v_{i,\mathrm{obs}} - v_{i,\mathrm{calc}}}{\sigma_i}\right]^2 + \left(\frac{v \sin i - 5.79 \text{ km s}^{-1} + 0.35 \text{ km s}^{-1} \times G(0,1)}{0.35 \text{ km s}^{-1}}\right)^2 + \left(\frac{P - 2.519\,9449 \text{ d} + 0.000\,0013 \text{ d} \times G(0,1)}{0.000\,0013 \text{ d}}\right)^2 + \left(\frac{T_0 - 54\,461.860\,99 + 0.000\,24 \times G(0,1)}{0.000\,24}\right)^2 + \left(\frac{R_p/R_* - 0.102\,71 + 0.000\,59 \times G(0,1)}{0.000\,59}\right)^2 + \left(\frac{a/R_* - 5.64 + 0.12 \times G(0,1)}{0.12}\right)^2 + \left(\frac{i_p - 88.^\circ7 + 1.^\circ15 \times G(0,1)}{1.^\circ15}\right)^2. \quad (2)$$

The fitted parameters and uncertainties are given in Table 5. Fig. 2 shows the data overplotted with the best-fitting model, $\lambda = -79.^\circ0^{+4.5}_{-4.3}$, and the model corresponding to an aligned orbit, $\lambda = 0^\circ$. It is obvious that the amplitude and symmetry of the observations do not match with the aligned model. We conclude that WASP-1b has a severely misaligned orbit with respect to the rotation axis of the host star.

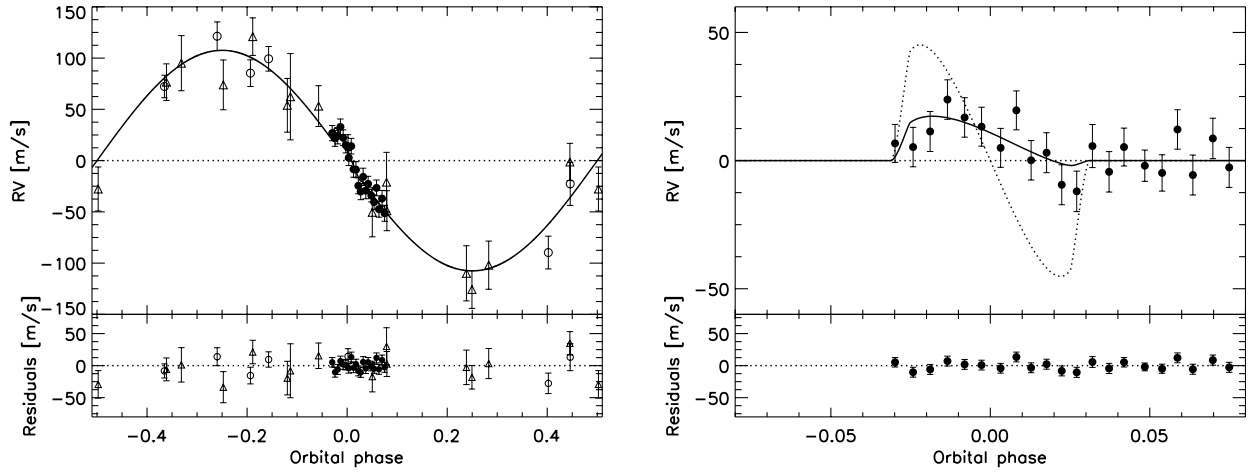

Figure 2. Left-hand panel: phase-folded radial velocities of WASP-1 minus the systematic velocity (given in Table 5), overplotted with the best-fitting model, with the residuals shown below. The orbital observations were taken using FIES (open triangles) and SOPHIE (open circles), and the transit sequence using SOPHIE (filled circles). Right-hand panel: spectroscopic transit minus the orbital velocity, overplotted with the best-fitting model ($\lambda = -79\overset{\circ}{.}0^{+4.5}_{-4.3}$, $v \sin i = 5.77 \pm 0.35$ km s^{-1}) and residuals shown below. The dotted line represents the RM effect of an aligned orbit.

The value of $v \sin i$ is constrained by the penalty function, and thus the uncertainty in λ is small despite the low impact parameter. It must be noted, however, that deriving $v \sin i$ from spectroscopic line broadening is susceptible to systematic errors due to the uncertainties in broadening mechanisms, such as microturbulence and macroturbulence, which are difficult to quantify. By altering $v \sin i$ by ± 1 km s^{-1}, we find that the best-fitting value of λ changes by no more than 5°, so the interpretation of a high obliquity is retained. The major factor leading the high precision in the determination of λ is the system geometry. In a system with a low impact parameter and large misalignment, the form of the RM effect changes rapidly with λ, so it easy to differentiate between different angles. Gaudi & Winn (2007) provide a relationship to estimate the expected uncertainty in λ. Substituting $\sigma_{\rm RV} = 8.5$ m s^{-1}, $N_{\rm obs} = 12$ and the derived values of $R_{\rm p}/R_*$, b, $v \sin i$ and λ into their equation (16), we obtain $\sigma_\lambda = 5\overset{\circ}{.}8$. This is in good agreement with the value we obtain and the small difference may due to the assumption that $v \sin i$ is a free parameter, whereas here we constrain it with the penalty function.

3.2 WASP-24

A transit of WASP-24b was observed with the HARPS spectrograph on the night of 2010 April 10. We acquired 51 spectra covering the full transit (161 min, 22 observations) and a period of duration 212 min (28 observations) distributed evenly before and after transit. The atmospheric conditions were stable and the seeing was 0.7 arcsec. We also obtained two observations on the nights prior to and post-transit to constrain the γ velocity of the transit data set.

To fit the orbital parameters, we obtained eight HARPS observations between 2010 March 26 and 28 and used 10 FIES and 18 CORALIE out-of-transit observations taken during the discovery of the planet (Street et al. 2010). The HARPS observations are given in Table 2.

Street et al. (2010) reported that the orbit is not eccentric, so e was fixed to 0. The linear limb-darkening coefficient was chosen from the tables of Claret (2004) (ATLAS models) for the V

Table 2. Radial velocities of WASP-24 measured with HARPS during and outside transit.

BJD − 240 0000	RV (km s^{-1})	Error (km s^{-1})
Planetary transit		
55296.6514	−17.7358	0.0059
55296.6651	−17.7463	0.0126
55296.6701	−17.7492	0.0118
55296.6750	−17.7407	0.0113
55296.6801	−17.7504	0.0112
55296.6850	−17.7733	0.0119
55296.6900	−17.7487	0.0119
55296.6950	−17.7436	0.0119
55296.7000	−17.7492	0.0124
55296.7051	−17.7629	0.0119
55296.7100	−17.7551	0.0123
55296.7150	−17.7619	0.0123
55296.7201	−17.7668	0.0121
55296.7250	−17.7521	0.0140
55296.7300	−17.7364	0.0131
55296.7350	−17.7379	0.0126
55296.7400	−17.7434	0.0123
55296.7450	−17.7512	0.0124
55296.7501	−17.7645	0.0118
55296.7550	−17.7403	0.0116
55296.7600	−17.7633	0.0119
55296.7650	−17.7531	0.0120
55296.7700	−17.8006	0.0122
55296.7751	−17.7885	0.0122
55296.7800	−17.7813	0.0115
55296.7851	−17.7965	0.0111
55296.7901	−17.8128	0.0109
55296.7950	−17.8160	0.0107
55296.8000	−17.8399	0.0098
55296.8049	−17.8265	0.0116
55296.8100	−17.8495	0.0121
55296.8150	−17.8366	0.0121
55296.8199	−17.8141	0.0139
55296.8251	−17.7952	0.0130
55296.8300	−17.8240	0.0129
55296.8350	−17.7943	0.0122

Table 2 – *continued*

BJD − 240 0000	RV (km s^{-1})	Error (km s^{-1})
55296.8401	−17.8418	0.0118
55296.8451	−17.8177	0.0112
55296.8500	−17.8012	0.0109
55296.8550	−17.8154	0.0108
55296.8600	−17.8018	0.0110
55296.8650	−17.8293	0.0110
55296.8701	−17.8289	0.0109
55296.8750	−17.8200	0.0110
55296.8801	−17.8355	0.0105
55296.8851	−17.8203	0.0108
55296.8901	−17.8294	0.0107
55296.8951	−17.8398	0.0100
55296.9000	−17.8602	0.0111
55296.9051	−17.8438	0.0116
55296.9101	−17.8287	0.0116
Other orbital phases		
55281.6933	−17.7475	0.0052
55281.9080	−17.6632	0.0045
55283.6945	−17.8572	0.0056
55283.9139	−17.7825	0.0045
55297.7382	−17.8696	0.0042
55297.9076	−17.8057	0.0043
55282.6762	−17.7674	0.0125
55282.6835	−17.7461	0.0118
55282.6911	−17.7431	0.0118
55282.6988	−17.7443	0.0141
55295.6485	−17.7747	0.0056
55295.9092	−17.6802	0.0039

Table 3. Radial velocities of WASP-38 measured with FIES during transit. The starred point (*) was omitted from the analysis.

HJD − 240 0000	RV (km s^{-1})	Error (km s^{-1})
55356.4021	−9.8108	0.0120
55356.4135	−9.8175	0.0084
55356.4248	−9.8113	0.0091
55356.4362	−9.8320	0.0057
55356.4476	−9.7805	0.0114
55356.4590	−9.7907	0.0069
55356.4704	−9.8042	0.0081
55356.4817	−9.7962	0.0074
55356.4931	−9.8042	0.0103
55356.5045	−9.8028	0.0089
55356.5159	−9.8149	0.0121
55356.5273	−9.8188	0.0010
55356.5386	−9.8072	0.0099
55356.5500*	−9.7912	0.0098
55356.5614	−9.8347	0.0074
55356.5728	−9.8802	0.0075
55356.5842	−9.8762	0.0106
55356.5956	−9.8841	0.0087
55356.6070	−9.9084	0.0089
55356.6183	−9.8734	0.0098
55356.6297	−9.8284	0.0081
55356.6411	−9.8365	0.0076
55356.6525	−9.8599	0.0102
55356.6639	−9.8602	0.0096
55356.6752	−9.8593	0.0083
55356.6866	−9.8661	0.0093
55356.6980	−9.8855	0.0122

filter and fixed at $u = 0.66$. Values of the photometric parameters P, T_0, R_p/R_*, a/R_* and i_p are taken from Street et al. (2010) and are constrained through the χ^2 fitting statistic below:

$$\chi^2 = \sum_i \left[\frac{v_{i,\mathrm{obs}} - v_{i,\mathrm{calc}}}{\sigma_i}\right]^2 + \left(\frac{P - 2.341\,2124\,\mathrm{d} + 0.000\,0020\,\mathrm{d} \times G(0,1)}{0.000\,0020\,\mathrm{d}}\right)^2 + \left(\frac{T_0 - 55\,081.379\,41 + 0.000\,17 \times G(0,1)}{0.000\,17}\right)^2 + \left(\frac{R_p/R_* - 0.100\,40 + 0.000\,60 \times G(0,1)}{0.000\,60}\right)^2 + \left(\frac{a/R_* - 5.90 + 0.33 \times G(0,1)}{0.33}\right)^2 + \left(\frac{i_p - 83.^\circ64 + 0.^\circ31 \times G(0,1)}{0.^\circ31}\right)^2. \quad (3)$$

Fig. 3 shows that WASP-24b has a very symmetrical RM effect, moving from redshift to blueshift. This implies that that the planet moves in a prograde, well-aligned orbit. A fit to the observations indicates the obliquity to be $\lambda = -4.^\circ7 \pm 4.^\circ0$. All the fitted parameters are shown in Table 6. The fitted value of $v \sin i = 7.32 \pm 0.88$ km s^{-1} matches very well with that found from spectral line fitting, $v \sin i = 7.0 \pm 1.0$ km s^{-1} (Street et al. 2010). WASP-24b has a high impact parameter ($b = 0.65$), so a penalty function on $v \sin i$ was not needed. We found that adding such a penalty function constraining $v \sin i$ to the value from Street et al. (2010) had no significant effect on the derived parameters.

3.3 WASP-38

The FIES spectrograph was employed to observe a transit of WASP-38b on 2010 June 8. We obtained 27 spectra during the night using an exposure time of 900 s, giving 16 in-transit and 12 out-of-transit observations (Table 3). The atmospheric conditions were stable and the seeing was 0.6 arcsec. To fit the orbit, we used the SOPHIE and CORALIE out-of-transit data from Barros et al. (2011). The CORALIE RV point at BJD = 245 5404.6205 was removed, as it occurred during transit. To obtain $\chi^2_{\mathrm{red}} = 1$, we required 15 and 8 m s^{-1} to be added in quadrature to the SOPHIE and CORALIE internal uncertainties, respectively.

Barros et al. (2011) found that WASP-38b has a small but significantly eccentric orbit, so we fixed $e = 0.0321$ and $\omega = -19^\circ$, since those parameters have little effect on the fitted parameters once the transit ephemeris is specified (Winn et al. 2011). The photometric parameters found from light-curve fitting (Barros et al. 2011) are constrained through the penalty function shown in equation (4). We determined the linear limb-darkening coefficient from the tables of Claret (2004) (ATLAS models) for the V filter and fixed $u = 0.64$.

Table 4. Radial velocities of HAT-P-8 measured with FIES during transit.

HJD − 240 0000	RV (km s^{-1})	Error (km s^{-1})
55440.4089	−22.2836	0.0067
55440.4203	−22.3043	0.0087
55440.4317	−22.3038	0.0078
55440.4431	−22.3326	0.0088
55440.4545	−22.3329	0.0141
55440.4658	−22.3481	0.0096
55440.4772	−22.3335	0.0114
55440.4886	−22.3029	0.0121
55440.5000	−22.3050	0.0156
55440.5114	−22.2710	0.0127
55440.5227	−22.2619	0.0134
55440.5341	−22.2827	0.0109
55440.5455	−22.3360	0.0139
55440.5632	−22.3694	0.0106
55440.5746	−22.3538	0.0105
55440.5860	−22.4051	0.0147
55440.5973	−22.4891	0.0126
55440.6087	−22.4947	0.0153
55440.6201	−22.4824	0.0132
55440.6315	−22.4606	0.0104
55440.6429	−22.4025	0.0132
55440.6542	−22.4083	0.0114
55440.6656	−22.3970	0.0128
55440.6770	−22.4072	0.0140
55440.6884	−22.4123	0.0137
55440.6998	−22.3928	0.0137
55440.7111	−22.3896	0.0122
55440.7225	−22.3998	0.0135

The impact parameter of WASP-38b is low and has a relatively large uncertainty, $b = 0.27^{+0.10}_{-0.14}$. As with WASP-1b, we require an independent constraint on $v \sin i$ to break the degeneracy between $v \sin i$ and λ. The values of the photometric parameters and $v \sin i = 8.6 \pm 0.4$ km s^{-1} are taken from Barros et al. (2011) and used in the χ^2 statistic:

$$\chi^2 = \sum_i \left[\frac{v_{i,\rm obs} - v_{i,\rm calc}}{\sigma_i}\right]^2 + \left(\frac{v \sin i - 8.69 \text{ km s}^{-1} + 0.40 \text{ km s}^{-1} \times G(0,1)}{0.40 \text{ km s}^{-1}}\right)^2 + \left(\frac{P - 6.871\,815 \text{ d} + 0.000\,045 \text{ d} \times G(0,1)}{0.000\,045 \text{ d}}\right)^2 + \left(\frac{T_0 - 55\,335.920\,50 + 0.000\,74 \times G(0,1)}{0.000\,74}\right)^2 + \left(\frac{R_{\rm p}/R_* - 0.0844 + 0.0011 \times G(0,1)}{0.0011}\right)^2 + \left(\frac{a/R_* - 12.15 + 0.19 \times G(0,1)}{0.19}\right)^2 + \left(\frac{i_{\rm p} - 88\overset{\circ}{.}69 + 0\overset{\circ}{.}67 \times G(0,1)}{0\overset{\circ}{.}67}\right)^2. \quad (4)$$

Although the precision of the RV measurements is lower than from the other spectrographs, we can see from the symmetry and characteristic redshift then blueshift of the RM effect that the planet is generally aligned and not retrograde. A fit to the data yields $\lambda = 15^{\circ}{}^{+33}_{-43}$, which is consistent with zero; the other fitted parameters are listed in Table 7. The large uncertainty in λ is due in part to the small differences in the shape of the RM effect when λ and b are small. Angles greater than $\sim 60^{\circ}$ produce a much more notable change in shape per degree than that at low angles, as shown in Fig. 4. Thus the data allow us to rule out very high misalignment angles; however, further observations are needed to reveal whether a small misalignment exists.

One observation lies more than 3σ from the best-fitting model (see the open triangle in Fig. 4). We investigated whether this could be due to an incorrect wavelength calibration, but this does not appear to be the cause. However, seeing changes or guiding issues may be factors. The fit is improved by removing the point, so it was excluded in the analysis. The best-fitting value of λ obtained when

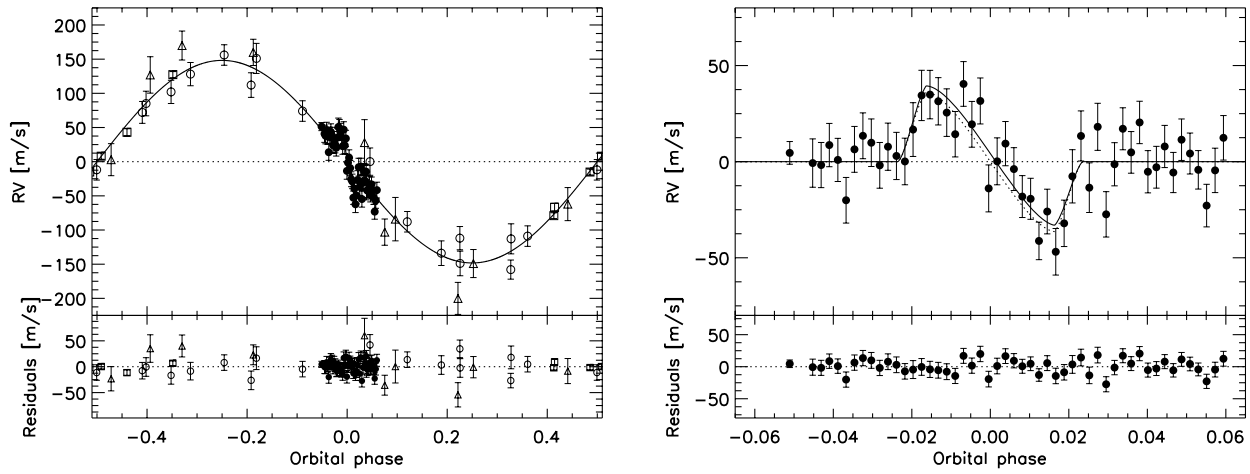

Figure 3. Left-hand panel: phase-folded radial velocities of WASP-24 overplotted with the best-fitting model. The systematic velocity has been removed (see Table 6) and the residuals are shown below. The orbital points were taken with FIES (open triangles), CORALE (open circles) and HARPS (open squares), and the HARPS transit sequence is shown in filled circles. Right-hand panel: the RM effect minus the orbital velocity is shown overplotted with the best-fitting model and that of an aligned orbit (dotted line). The residuals are plotted below.

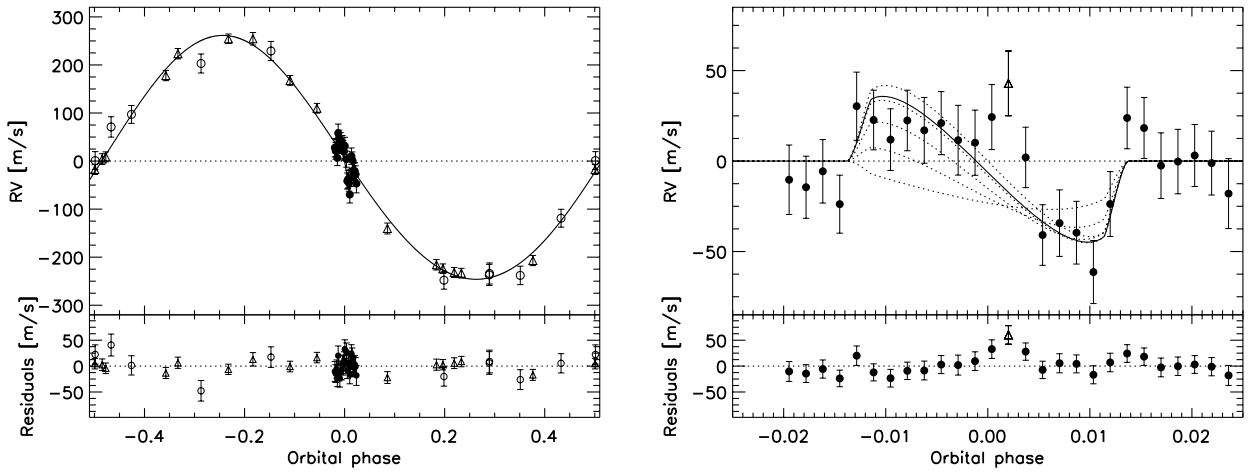

Figure 4. Left-hand panel: phase-folded radial velocities of WASP-38 overplotted with the best-fitting model. The systematic velocity has been removed (see Table 7) and the residuals are shown below. The orbital points were taken with SOPHIE (open circles) and CORALE (open triangles), and the FIES transit sequence is shown in filled circles. Right-hand panel: the spectroscopic transit is shown minus the orbital velocity and overplotted with the best-fitting model. The point represented by an open triangle was omitted from the analysis (see text). The dotted lines represent the models for $\lambda = 0^\circ$, 20°, 40°, 60° and 80° (from top to bottom) showing the change in the shape of the RM effect with λ. The residuals from the best-fitting model are shown below.

the discrepant point is retained is $-42^{\circ+32}_{-13}$, which is not inconsistent with zero at the 1.3σ level.

3.4 HAT-P-8

We observed a transit of HAT-P-8b with the FIES spectrograph on 2010 August 31. An exposure time of 900 s was used to obtain 14 in-transit and 14 out-of-transit spectra (Table 4). The seeing was 0.55 arcsec and weather conditions were good. Between the sixth and seventh in-transit observations, the telescope was repointed when the rotator reached the maximum limit, which required ∼9 min but did not affect the quality of the data set. We used the HIRES out-of-transit RV points from Latham et al. (2009) to constrain the orbit and fixed the eccentricity of the orbit to zero. The linear limb-darkening coefficient was set to the value found from the tables of Claret (2004) (ATLAS models) for the V filter, $u = 0.69$.

Discovery light curves of HAT-P-8b were taken in 2007, so in order to improve the accuracy of the ephemeris, we fitted the two full z-band light curve presented in Latham et al. (2009) and a high-quality transit taken on 2010 August 28 by F. Harmuth (TRESCA/ETD), as shown in Fig. 5. The TRESCA observations were taken using the 1.2-m telescope at the Calar Alto Observatory in the R band. As with WASP-1b, an MCMC routine was used to fit the data, and the parameters found for P, T_0, R_p/R_*, a/R_* and i_p are shown in equation (6).

An initial fit to the RM data found $v \sin i \sim 16\,\mathrm{km\,s^{-1}}$ (and $\lambda \sim 8^\circ$) to be significantly larger than the value of $v \sin i = 11.5 \pm 0.5\,\mathrm{km\,s^{-1}}$ reported by Latham et al. (2009). Other similarly fast rotating stars have also been found to show a discrepancy between the value of $v \sin i$ derived from spectroscopic line broadening and from RM measurements (e.g. Winn et al. 2007; Triaud et al. 2009). It is likely to be the result of the assumption that the line profile asymmetry caused by the planet blocking the rotating stellar surface can be modelled as a shift in the mean line position. For faster rotating stars, the asymmetry in the line profile is better resolved because of the broader linewidth, which causes a larger apparent shift than expected, as seen here. Hirano et al. (2010) have addressed this issue by modifying the equations presented in Ohta et al. (2005)

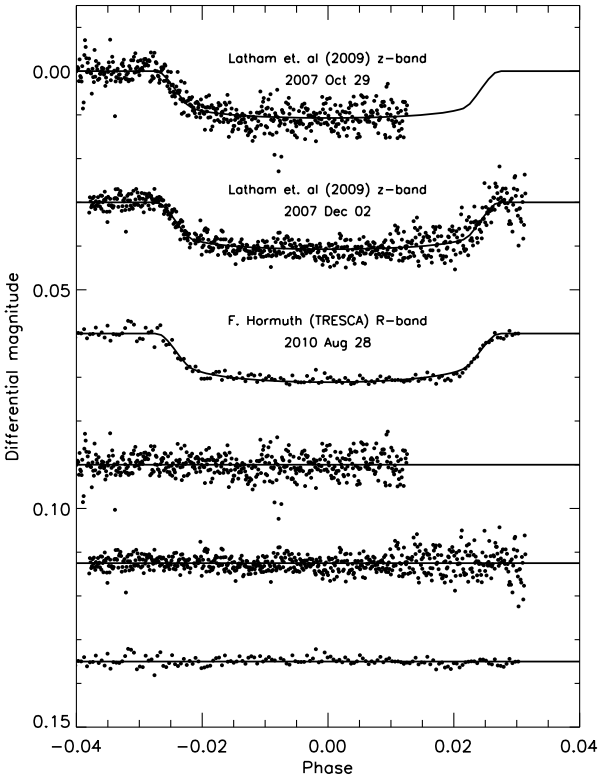

Figure 5. Photometry of three transits of HAT-P-8b and the residuals from the best-fitting model.

to compensate for this effect. We implemented this solution as in Simpson et al. (2010a) and Bayliss et al. (2010) by calculating the RM RV shift as

$$v_{\mathrm{RM}} = -\delta v_{\mathrm{p}} \left[1 + \frac{\sigma^2}{2\beta^2 + \sigma^2}\right]^{3/2} \left[1 - \frac{v_{\mathrm{p}}^2}{2\beta^2 + \sigma^2}\right], \quad (5)$$

where β is the intrinsic linewidth and $\sigma = v \sin i/\alpha$, where α is a scaling factor depending on limb-darkening parameters (see equation F6 of H09). We determined β as the quadrature sum of

the macroturbulence ($v_{\rm mac}$), microturbulence ($v_{\rm mic}$) and instrumental profile. Following Valenti & Fischer (2005), we used $v_{\rm mac} = 4.60\,{\rm km\,s^{-1}}$ and $v_{\rm mic} = 0.85\,{\rm km\,s^{-1}}$. The instrumental profile is given by $c/R = 6.38\,{\rm km\,s^{-1}}$, where R is the instrumental resolution 46 000. Thus we determined $\beta = 7.9\,{\rm km\,s^{-1}}$. We calculated $\alpha = 1.31$ for the limb-darkening coefficients $u_1 = 0.69$ and $u_2 = 0$.

As with WASP-1b and WASP-38b, HAT-P-8b has a low impact parameter, and therefore we placed a penalty function on the value of $v \sin i$ found by Latham et al. (2009) to constrain the fit. The χ^2 statistic used was

$$\chi^2 = \sum_i \left[\frac{v_{i,\rm obs} - v_{i,\rm calc}}{\sigma_i}\right]^2 + \left(\frac{v\sin i - 11.5\ {\rm km\,s^{-1}} + 0.5\ {\rm km\,s^{-1}} \times G(0,1)}{0.5\ {\rm km\,s^{-1}}}\right)^2 + \left(\frac{P - 3.076\,3350{\rm d} + 0.000\,0040{\rm d} \times G(0,1)}{0.000\,0040\,{\rm d}}\right)^2 + \left(\frac{T_0 - 54\,437.675\,82 + 0.000\,34 \times G(0,1)}{0.000\,34}\right)^2 + \left(\frac{R_{\rm p}/R_* - 0.091\,10 + 0.000\,90 \times G(0,1)}{0.000\,90}\right)^2 + \left(\frac{a/R_* - 6.35 + 0.34 \times G(0,1)}{0.34}\right)^2 + \left(\frac{i_{\rm p} - 87\overset{\circ}{.}26 + 1\overset{\circ}{.}00 \times G(0,1)}{1\overset{\circ}{.}00}\right)^2. \quad (6)$$

From the form of the RM effect, HAT-P-8b appears to have a prograde aligned orbit, as shown in Fig. 6. A fit to the data yields $\lambda = -9\overset{\circ}{.}7^{+9.0}_{-7.7}$, and the other fitted parameters are shown in Table 8. As with WASP-38b, the precision of FIES and the combination of low b and λ limit the accuracy of the result, but allow us to rule out highly misaligned orbits. A transit of HAT-P-8b was independently observed with SOPHIE (Moutou et al., in preparation); it provides results similar to the ones presented here.

Two observations show a large deviation from the best-fitting model and again we could not determine an instrumental cause. We found that the fit was not significantly altered nor improved by removing the points so chose to retain them. The best-fitting value of λ having removed the two points ($-18^\circ \pm 11^\circ$) is consistent with that found if the points are retained.

4 CONCLUSIONS

The spectroscopic transits of WASP-1b, WASP-24b, WASP-38b and HAT-P-8b have been observed using the HARPS, SOPHIE and FIES spectrographs. We modelled the RM effects and found the sky projected spin-orbit alignment angle of the systems to be $\lambda = -79\overset{\circ}{.}0^{+4.5}_{-4.3}$, $-4\overset{\circ}{.}7 \pm 4\overset{\circ}{.}0$, $15^{\circ}{}^{+33}_{-43}$ and $-9\overset{\circ}{.}7^{+9.0}_{-7.7}$, respectively. WASP-24b, WASP-38b and HAT-P-8b do not appear to be strongly misaligned and are consistent with zero within 2σ. This suggests they could have undergone a relatively non-violent migration process which did not perturb them from the primordial alignment of the protoplanetary disc. Alternatively, tidal interactions may have forced the stellar spin to align with the planetary orbit (Winn et al. 2010a). By contrast, WASP-1b joins the approximately one-third of planets with misaligned orbits and points towards a dynamically violent evolution such as gravitational scattering by other planets or the three-body Kozai mechanism.

The uncertainties in λ for HAT-P-8b and particularly WASP-38b are relatively large and allow for the possibility that the systems have a small misalignment. These larger uncertainties are due, in part, to the geometry of the systems. Both planets have low impact parameters, and in this regime the shape of the RM effect, which largely determines λ, changes very subtly with λ until angles of $\gtrsim 60^\circ$ are reached. Thus, many values of λ can be fitted by the data and the uncertainty is large. This explains how we are able to obtain a much more precise value for WASP-1b which has a value of $|\lambda|$ which is much greater than zero. In addition, we are also limited by the instrumental noise on the FIES spectrograph, and we recommend that further observations of these systems be undertaken to refine the parameters.

We modelled the RM effect using the equations of Ohta et al. (2005). However, it has been shown that this formulation does not estimate $v \sin i$ well for more rapidly rotating stars. We found this to be the case for HAT-P-8, which was measured to have $v \sin i = 11.5 \pm 0.5\,{\rm km\,s^{-1}}$ from spectroscopic line broadening but a best-fitting value of $16\,{\rm km\,s^{-1}}$ from the RM effect. For this case, we

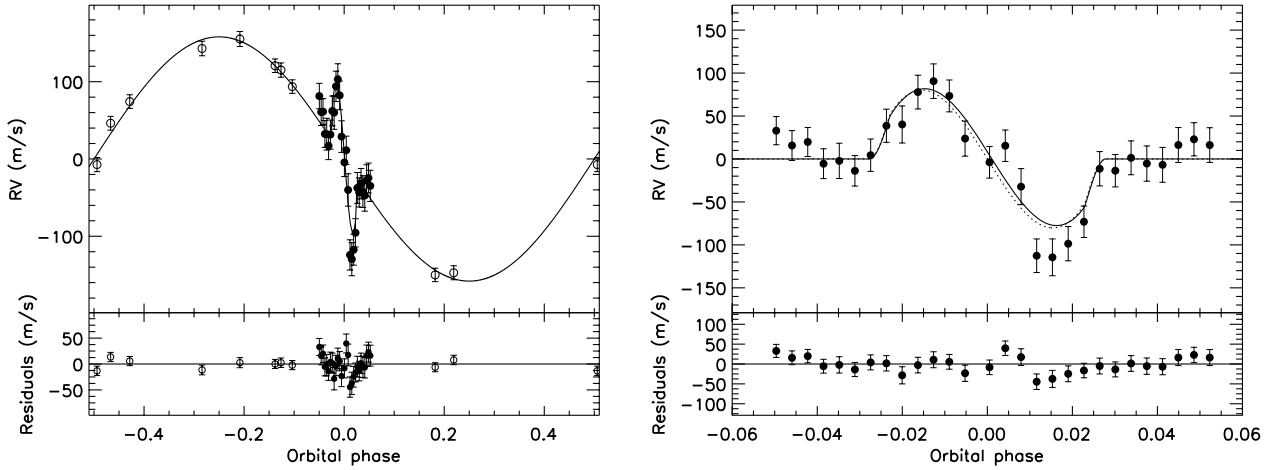

Figure 6. Left-hand panel: phase-folded radial velocities of HAT-P-8 minus the systematic velocity (given in Table 8) and overplotted with the best-fitting model with residuals shown below. The orbital observations were taken using HIRES (open circles), and the transit sequence using FIES (filled circles). Bottom panel: the spectroscopic transit, minus the orbital velocity, is shown overplotted with the best-fitting model with the residuals shown below. A dotted line represents the RM effect of an aligned orbit.

used the modified formulation of Hirano et al. (2010) to model the data and placed a constraint on $v \sin i$ using the value from spectroscopic line broadening to break the degeneracy between λ and $v \sin i$ at low impact parameters. These modifications did not affect the conclusion that HAT-P-8b appears to be well aligned.

The RM effect allows us to measure the spin-orbit angle in the plane of the sky. However, the line-of-sight alignment can be estimated by comparing the inclinations of the planetary orbit and stellar rotation axes $i_{\rm p}$ and i_*. Transiting planets naturally provide a tight constraint on $i_{\rm p}$ given that the orbit must be close to edge-on in order for an eclipse to be observed. The stellar spin axis is more difficult to obtain and may be inferred by comparing the line-of-sight rotational velocity, $v \sin i$, to the true stellar rotation velocity v. Theoretical predictions of v are provided by Schlaufman (2010) for many of the host stars of transiting planets; however, the error budget is large due to observational and model uncertainties. It can also be determined through the relation $v = 2\pi R_*/P_{\rm rot}$, where $P_{\rm rot}$, the stellar rotation period, can be measured directly from spot modulation (e.g. Baliunas et al. 1997; Simpson et al. 2010b) or indirectly from Ca II H&K measurements (Noyes et al. 1984; Watson et al. 2010a) if this information is available. This method also has large uncertainties associated with it because the stellar rotation

Table 5. Derived system parameters and uncertainties for WASP-1b. The values used in the χ^2 fitting statistic in equation (2) are taken from previous observations and are used to constrain the explored parameter space during the fit. These parameters are allowed to float during the procedure in order to propagate the associated uncertainty. Thus the derived parameter values and uncertainties given in this table differ slightly from the input values because of the influence of the RM data. The effective temperature is taken from Stempels et al. (2007).

Parameter (units)	Symbol	Value
Free parameters		
Projected alignment angle (°)	λ	$-79.0^{+4.5}_{-4.3}$
RV semi-amplitude (km s^{-1})	K	$0.1094 \pm 0.005\,64$
Systemic velocity of SOPHIE transit data set (km s^{-1})	γ_1	-13.5016 ± 0.0065
Systemic velocity of SOPHIE orbital data set (km s^{-1})	γ_2	-13.5016 ± 0.0065
Systemic velocity of FIES orbital data set (km s^{-1})	γ_3	-13.4990 ± 0.0057
Parameters controlled by priors		
Projected stellar rotation velocity (km s^{-1})	$v \sin i$	5.77 ± 0.35
Period (d)	P	$2.519\,9449 \pm 0.000\,0013$
Transit epoch (HJD − 240 0000)	T_0	$54\,461.860\,99 \pm 0.000\,24$
Planet/star radius ratio	$R_{\rm p}/R_*$	$0.102\,71 \pm 0.000\,58$
Scaled semimajor axis	a/R_*	5.64 ± 0.13
Orbital inclination (°)	i	$88.65^{+0.51}_{-0.55}$
Fixed parameters		
Eccentricity	e	0
Limb darkening	u	0.73
Effective temperature (K)	$T_{\rm eff}$	6110 ± 45

Table 6. Derived system parameters and uncertainties for WASP-24b. The effective temperature is taken from Street et al. (2010). Please see the caption in Table 5.

Parameter (units)	Symbol	Value
Free parameters		
Projected alignment angle (°)	λ	-4.7 ± 4.0
Projected stellar rotation velocity (km s^{-1})	$v \sin i$	7.0 ± 0.9
RV semi-amplitude (km s^{-1})	K	0.1482 ± 0.0025
Systemic velocity of HARPS transit data set (km s^{-1})	γ_1	-17.7871 ± 0.0017
Systemic velocity of HARPS orbital data set (km s^{-1})	γ_2	-17.7905 ± 0.0019
Systemic velocity of FIES orbital data set (km s^{-1})	γ_3	-17.9050 ± 0.0073
Systemic velocity of CORALIE orbital data set (km s^{-1})	γ_4	-17.8031 ± 0.0040
Parameters controlled by priors		
Period (d)	P	$2.341\,2127 \pm 0.000\,0020$
Transit epoch (HJD − 240 0000)	T_0	$55\,081.379\,41 \pm 0.000\,17$
Planet/star radius ratio	$R_{\rm p}/R_*$	$0.100\,40 \pm 0.000\,60$
Scaled semimajor axis	a/R_*	5.98 ± 0.15
Orbital inclination (°)	i	83.64 ± 0.29
Fixed parameters		
Eccentricity	e	0
Limb darkening	u	0.66
Effective temperature (K)	$T_{\rm eff}$	6075 ± 100

Table 7. Derived system parameters and uncertainties for WASP-38b. The effective temperature is taken from Barros et al. (2011). Please see the caption in Table 5.

Parameter (units)	Symbol	Value
Projected alignment angle (°)	λ	15^{+33}_{-43}
RV semi-amplitude (km s^{-1})	K	0.2538 ± 0.0035
Systemic velocity of FIES transit data set (km s^{-1})	γ_1	$-9.8404^{+0.0053}_{-0.0057}$
Systemic velocity of SOPHIE orbital data set (km s^{-1})	γ_2	-9.7181 ± 0.0063
Systemic velocity of CORALIE orbital data set (km s^{-1})	γ_3	-9.7951 ± 0.0027
Parameters controlled by priors		
Projected stellar rotation velocity (km s^{-1})	$v \sin i$	8.58 ± 0.39
Period (d)	P	$6.871\,814 \pm 0.000\,045$
Transit epoch (HJD − 240 0000)	T_0	$55\,335.920\,44 \pm 0.000\,74$
Planet/star radius ratio	R_p/R_*	0.0844 ± 0.0011
Scaled semimajor axis	a/R_*	12.15 ± 0.18
Orbital inclination (°)	i	$88.83^{+0.51}_{-0.55}$
Fixed parameters		
Eccentricity	e	0.032
Longitude of periastron	ω	−19.0
Limb darkening	u	0.64
Effective temperature (K)	$T_{\rm eff}$	6150 ± 80

Table 8. Derived system parameters and uncertainties for HAT-P-8. The effective temperature is taken from Latham et al. (2009). Please see the caption in Table 5.

Parameter (units)	Symbol	Value
Free parameters		
Projected alignment angle (°)	λ	$-9.7^{+9.0}_{-7.7}$
RV semi-amplitude (km s^{-1})	K	0.1580 ± 0.0041
Systemic velocity of FIES transit data set (km s^{-1})	γ_1	-22.3650 ± 0.0040
Systemic velocity of HIRES orbital data set (km s^{-1})	γ_2	-0.0937 ± 0.0031
Parameters controlled by priors		
Projected stellar rotation velocity (km s^{-1})	$v \sin i$	11.8 ± 0.5
Period (d)	P	$3.076\,3370 \pm 0.000\,0036$
Transit epoch (HJD − 240 0000)	T_0	$54\,437.675\,87 \pm 0.000\,34$
Planet/Star radius ratio	R_p/R_*	$0.091\,35 \pm 0.000\,89$
Scaled semimajor axis	a/R_*	$6.12^{+0.20}_{-0.21}$
Orbital inclination (°)	i	$87.80^{+0.75}_{-0.77}$
Fixed parameters		
Eccentricity	e	0
Limb darkening	u	0.69
Effective temperature (K)	$T_{\rm eff}$	6200 ± 80

period varies across the surface, for example due to differential rotation. The rotational velocity of the plasma is also different inside a spot and outside of it (Lustig & Woehl 1993); thus, the derived rotation period depends on the type and position of spot used for the analysis.

The four stars in this study have similar values of $T_{\rm eff}$ (see Tables 5–8) and age (see Schlaufman 2010), so we would expect them to have comparable values of v. Schlaufman (2010) predicts this to be of the order of 7–9 km s^{-1}. In practice, we find a wide range of values of $v \sin i$: 5.77 ± 0.35; 7.32 ± 0.88, 8.58 ± 0.39 and 11.8 ± 0.5 km s^{-1}. This can be explained by supposing that the slower rotating stars are tilted so that we only measure a fraction of the true rotational velocity. WASP-1 is slower rotating than predicted ($v \sin i = 5.8$ km s^{-1}, $v_{\rm sim} = 8.6$ km s^{-1}), and from this, Schlaufman (2010) deduced that the star and planet are significantly misaligned in the line of sight. This method yields four solutions for the inclination of the rotation axis of the star, $i_* \sim 40°$, $140°$, $220°$ and $320°$.

The total alignment angle can be calculated through the following relation:

$$\cos\psi = \cos i_* \cos i_{\rm p} + \sin i_* \sin i_{\rm p} \cos\lambda. \quad (7)$$

Substituting $i_{\rm p} = 88.^{\circ}6$ and $\lambda = -79°$, we obtain $\psi = 82°, 84°, 96°$ and $98°$. We therefore conclude that WASP-1b has an almost polar orbit. Schlaufman (2010) did not find WASP-24b and HAT-P-8b to have highly misaligned orbits in the line of sight, and WASP-38b has a similar $v \sin i$, so we do not expect it to be misaligned either. This agrees with the lack of evidence for strong misalignments in the plane of the sky from the RM effect in these systems.

Previous authors have noted correlations between spin-orbit misalignment, eccentric orbits and massive planets (see Fig. 7, and fig. 9 of Hébrard et al. 2010). With $e = 0.032$ and $m_{\rm p} = 2.7 M_{\rm J}$,

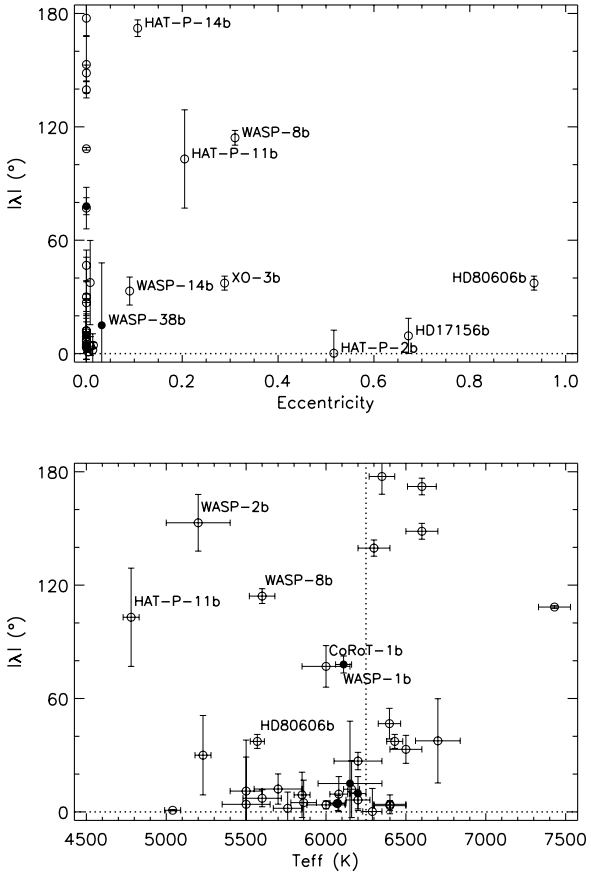

Figure 7. Top panel: the absolute value of the spin-orbit angle, λ, versus orbital eccentricity. Whilst the majority of eccentric planets are misaligned, there are also many circular misaligned systems. The four planets in this analysis are shown as filled points. Bottom panel: the absolute value of the spin-orbit angle versus stellar effective temperature, showing a correlation between misalignment and $T_{\rm eff} > 6250$ K as proposed by Winn et al. (2010a). In their analysis, WASP-2b and CoRoT-1b were removed due to large uncertainties, and WASP-8b, HD 80606b and HAT-P-11b were deemed exceptions due to their long tidal evolution time-scales caused by long orbital period or low planet mass.

WASP-38b may be expected to be misaligned; however, we find no evidence for high spin-orbit angles.

Winn et al. (2010a) noted that planets orbiting hot stars, defined as $T_{\rm eff} > 6250$ K, tend to have misaligned orbits, whereas stars cooler than this host aligned planets, as shown in Fig. 7. Low-mass and long-period planets are exceptions, as the time-scale for tidal alignment is longer and may not have taken effect. All the planets in this study have temperatures placing them in the cool star category and so WASP-24b, WASP-38b and HAT-P-8b appear to conform with this trend. However, with its $\sim$7 d orbit, WASP-38b has the potential to be an exception and to have retained its primordial spin-orbit angle.

By contrast, the WASP-1 system, with $T_{\rm eff} = 6110 \pm 45$ K, is unexpectedly misaligned. In this way, WASP-1b is similar to CoRoT-1b, which also orbits a cool star, $T_{\rm eff} = 5950 \pm 150$ K (Barge et al. 2008), and has a highly misaligned, almost polar orbit, $\lambda = 77^\circ \pm 11^\circ$ (Pont et al. 2010), yet is not eccentric. Neither planets are low mass nor long period, so do not meet the criteria to be exceptions from aligned orbits around cool stars. To bring the stars into the hot-star regime, the temperatures of CoRoT-1 and WASP-1 would have to be several σ hotter than their best-fitting values. Whilst this could be the case, another possibility is that the distinction between cool and hot stars is not discrete, and there may be a transition region between the two.

Interestingly, Cameron et al. (2007) reported a nearby stellar companion to WASP-1, and if associated, would have a projected orbital separation of $\sim$1800 AU. In this regime, the Kozai mechanism can take effect, and it is thought to significantly perturb planetary orbits. Although beyond the scope of this paper, it would be very informative to investigate whether the migration of WASP-1b could have been caused by interactions with a binary companion, if it is indeed associated.

The rapid increase in the number of measured spin-orbit angles, and the discovery of a large population of misaligned systems, has revolutionized our understanding of planetary migration. It is no longer believed that planet–disc interactions can fully explain the observed distribution of angles and other mechanisms must play a significant role. In this paper, we have presented four new measurements of spin-orbit angles and we find that WASP-1b has a near polar orbit, despite predictions that it would be aligned as it orbits a cool star. By contrast, WASP-38b is a massive planet on a moderately long period, eccentric orbit so has a high likelihood of misalignment, but it does not show evidence for a large obliquity. In order to fully understand the processes which are at work, further measurements are needed to allow theories to be compared with a strong observational basis. Morton & Johnson (2011) estimate that a total of 40–100 measurements will be required to be confident in the mechanisms at work, and with the steady flow of new transiting planet discoveries, uncovering the mystery of migration may soon be within our reach.

ACKNOWLEDGMENTS

We thank J. Southworth for making available his code, JKTLD, for calculating theoretical limb-darkening coefficients. FPK is grateful to AWE Aldermaston for the award of a William Penny Fellowship.

REFERENCES

Albrecht S., Winn J. N., Carter J. A., Snellen I. A. G., de Mooij E. J. W., 2011, ApJ, 726, 68
Baliunas S. L., Henry G. W., Donahue R. A., Fekel F. C., Soon W. H., 1997, ApJ, 474, L119
Baranne A. et al., 1996, A&AS, 119, 373
Barge P. et al., 2008, A&A, 482, L17
Barros S. C. C. et al., 2011, A&A, 525, A54
Bate M. R., Lodato G., Pringle J. E., 2010, MNRAS, 401, 1505
Bayliss D. D. R., Winn J. N., Mardling R. A., Sackett P. D., 2010, ApJ, 722, L224
Bouchy F., Hébrard G., Udry S., Delfosse X., Boisse I. E., 2009, A&A, 505, 853
Buchhave L. A. et al., 2010, ApJ, 720, 1118
Butler R. P., Marcy G. W., 1996, ApJ, 464, L153
Cameron A. C. et al., 2007, MNRAS, 375, 951
Charbonneau D., Winn J. N., Everett M. E., Lathoun D. W., Holman M. J., Esquero G. A., O'Donovan F. T., 2007, ApJ, 658, 1322
Claret A., 2004, A&A, 428, 1001
Fabrycky D. C., Winn J. N., 2009, ApJ, 696, 1230
Gaudi B. S., Winn J. N., 2007, ApJ, 655, 550
Gillon M., 2009, preprint (arXiv:0906.4904)
Hébrard G. et al., 2008, A&A, 488, 763
Hébrard G. et al., 2010, A&A, 516, A95
Hirano T., Suto Y., Taruya A., Narita N., Sato B., Johnson J. A., Winn J. N., 2010, ApJ, 709, 485

Johnson J. A., Winn J. N., Albrecht S., Howard A. W., Marcy G. W., Gazak J. Z., 2009, PASP, 121, 1104
Lai D., Foucart F., Lin D. N. C., 2011, MNRAS, 412, 2790
Latham D. W. et al., 2009, ApJ, 704, 1107
Lin D. N. C., Bodenheimer P., Richardson D. C., 1996, Nat, 380, 606
Loeillet B. et al., 2008, A&A, 481, 529
Lovis C., Pepe F., 2007, A&A, 468, 1115
Lustig G., Woehl H., 1993, A&A, 278, 637
McLaughlin D. B., 1924, ApJ, 60, 22
Marcy G. W., Butler R. P., 1996, ApJ, 464, L147
Markwardt C. B., 2009, in Bohlender D. A., Durand D., Dowler P., eds, ASP Conf. Ser. Vol. 411, Astronomical Data Analysis Software and Systems XVIII. Astron. Soc. Pac., San Francisco, p. 251
Mayor M., Queloz D., 1995, Nat, 378, 355
Mayor M. et al., 2003, Messenger, 114, 20
Morton T. D., Johnson J. A., 2011, ApJ, 729, 138
Moutou C., Hébrard G., Bouchy F., Eggenberger A., Boisse I., 2009, A&A, 498, L5
Murray N., Hansen B., Holman M., Tremaine S., 1998, Sci, 279, 69
Nagasawa M., Ida S., Bessho T., 2008, ApJ, 678, 498
Narita N. et al., 2009, PASJ, 61, 991
Noyes R. W., Hartmann L. W., Baliunas S. L., Duncan D. K., Vaughan A. H., 1984, ApJ, 279, 763
Ohta Y., Taruya A., Suto Y., 2005, ApJ, 622, 1118
Pepe F., Mayor M., Galland F., Naef D., Queloz D., Santos N. C., Udry S., Burnat M., 2002, A&A, 388, 632
Perruchot S. et al., 2008, in McLean I. S., Casali M. M., eds, Proc. SPIE Conf. Ser. Vol. 7014, Ground-based Instrumentation for Astronomy. SPIE, Bellingham, p. 17
Poddaný S., Brát L., Pejcha O., 2010, New Astron., 15, 297
Pollacco D. et al., 2008, MNRAS, 385, 1576
Pont F. et al., 2009, A&A, 502, 695
Pont F. et al., 2010, MNRAS, 402, L1
Queloz D., Casse M., Mayor M., 1999, in Hearnshaw J. B., Scarfe C. D., eds, ASP Conf. Ser. Vol. 185, IAU Colloq. 170, Precise Stellar Radial Velocities. Astron. Soc. Pac., San Francisco, p. 13
Queloz D. et al., 2010, A&A, 517, L1
Rasio F. A., Ford E. B., 1996, Sci, 274, 954
Rossiter R. A., 1924, ApJ, 60, 15
Rupprecht G. et al., 2004, in Moorwood A. F. M., Iye M., eds, Proc. SPIE Conf. Ser. Vol. 5492, Ground-based Instrumentation for Astronomy. SPIE, Bellingham, p. 148
Schlaufman K. C., 2010, ApJ, 719, 602
Shporer A., Tamuz O., Zucker S., Mazeh T., 2007, MNRAS, 376, 1296
Simpson E. K. et al., 2010a, MNRAS, 405, 1867
Simpson E. K., Baliunas S. L., Henry G. W., Watson C. A., 2010b, MNRAS, 408, 1666
Stempels H. C., Collier Cameron A., Hebb L., Smalley B., Frandsen S., 2007, MNRAS, 379, 773
Street R. A. et al., 2010, ApJ, 720, 337
Triaud A. H. M. J. et al., 2009, A&A, 506, 377
Triaud A. H. M. J. et al., 2010, A&A, 524, 25
Valenti J. A., Fischer D. A., 2005, ApJS, 159, 141
Watson C. A., Littlefair S. P., Cameron A. C., Dhillon V. S., Simpson E. K., 2010a, MNRAS, 408, 1606
Watson C. A. et al., 2010b, ArXiv e-prints
Wheatley P. J. et al., 2010, preprint (arXiv:1004.0836)
Winn J. N. et al., 2007, ApJ, 665, L167
Winn J. N. et al., 2009, ApJ, 703, 2091
Winn J. N., Fabrycky D., Albrecht S., Johnson J. A., 2010a, ApJ, 718, L145
Winn J. N. et al., 2010b, ApJ, 723, L223
Winn J. N. et al., 2011, AJ, 141, 63
Wu Y., Murray N., 2003, ApJ, 589, 605

This paper has been typeset from a TEX/LATEX file prepared by the author.